Available online at www.sciencedirect.com

ScienceDirect

Advances in Space Research xxx (xxxx) xxx

ADVANCES IN SPACE RESEARCH (a COSPAR publication)

www.elsevier.com/locate/asr

# Electron density fluctuations from Swarm as a proxy for ground-based scintillation data: A statistical perspective

Daria Kotova [a,*], Yaqi Jin [a], Luca Spogli [b,c], Alan G. Wood [d], Jaroslav Urbar [b,e], James T. Rawlings [f], Ian C. Whittaker [f], Lucilla Alfonsi [b], Lasse B.N. Clausen [a], Per Høeg [a], Wojciech J. Miloch [a]

[a] Department of Physics, University of Oslo, PO Box 1048, Blindern, Oslo 0316, Norway
[b] Istituto Nazionale di Geofisica e Vulcanologia, Via di Vigna Murata, 605, Rome 00143, Italy
[c] SpacEarth Technology, Via di Vigna Murata, 605, Rome 00143, Italy
[d] Space Environment and Radio Engineering Group (SERENE), University of Birmingham, 142 Edgbaston Park Rd, Birmingham B15 2TT, UK
[e] Institute of Atmospheric Physics CAS, Bocni II 1401, Prague 141 00, Czech Republic
[f] Department of Physics & Mathematics, Nottingham Trent University, Clifton, Nottinghamshire, NG11 8NS, UK

Received 4 February 2022; received in revised form 18 November 2022; accepted 21 November 2022

**Abstract**

The Swarm satellite mission has been used for numerous studies of the ionosphere. Here we use a global product, based on electron density measurements from Swarm that characterises ionospheric variability. The IPIR (Ionospheric Plasma IRregularities product) provides characteristics of plasma irregularities in terms of their amplitudes, gradients and spatial scales and assigns them to geomagnetic regions. Ionospheric irregularities and fluctuations are often the cause of errors in position, navigation, and timing (PNT) based on the Global Navigation Satellite Systems (GNSS), in which signals pass through the ionosphere. The IPIR dataset also provides an indication, in the form of a numerical value index (IPIR index), of the severity of irregularities affecting the integrity of *trans*-ionospheric radio signals and hence, the accuracy of GNSS positioning. We analysed datasets from Swarm A and ground-based scintillation receivers. Time intervals (when Swarm A passes over the field of view of the ground-based GPS receiver) are compared to ground-based scintillation data, collecting an azimuthal selection of the GNSS data relevant to the Swarm satellite overpass. We provide validations of the IPIR product against the ground-based measurements from 23 ground-based receivers, focusing on GPS TEC and scintillation data in low-latitude, auroral and polar regions, and in different longitudinal sectors. We have determined the median, mean, maximum and standard deviation of the parameter values for both datasets and each conjunction point. We found a weak correlation of the intensity of both phase and amplitude scintillation with the IPIR index.


*Keywords:* Amplitude and phase scintillations; Ionospheric irregularities; Polar cap, cusp, auroral and equatorial regions; Space weather; In-situ plasma density from low-earth orbit satellite; Topside ionosphere

## 1. Introduction

Ionospheric plasma is often characterised by irregularities and fluctuations in its density. They are the result of and reflect complex interactions in the near-Earth space environment due to the coupling of the solar wind, magnetosphere, ionosphere, and thermosphere (Kelley, 2009). Plasma density irregularities and fluctuations can influence the propagation of *trans*-ionospheric radio waves and thus are of importance for ground-based operations that rely on precise positioning with Global Navigation Satellite Sys-

* Corresponding author.
*E-mail address:* daria.kotova@fys.uio.no (D. Kotova).

https://doi.org/10.1016/j.asr.2022.11.042
0273-1177/

tems (GNSS) (Kintner et al., 2007). This consequently leads to scintillations in the phase and amplitude of the received radio wave (Yeh and Liu, 1982). Ionospheric scintillation is related to rapid variations in received amplitude and phase of radio waves transiting the ionosphere due to the presence of small-scale plasma density irregularities along the ray path. In the ionosphere, smaller-scale structures can arise from steep plasma density gradients (e.g., at the edge of larger-scale structures) due to instability processes such as the gradient-drift instability (GDI) and/or the velocity shear driven instability (Kelvin-Helmholtz instability, KHI), with energy cascading from larger to smaller scales in the plasma density (Keskinen & Ossakow, 1983). In extreme cases, scattering of the radio waves can result in the observer's view of the radio source being entirely lost, completely disrupting radio communication through the ionosphere and radio astronomy observations. Hence, the quality of navigation services relying on radio signals, such as the *trans*-ionospheric radio signals of GNSS, can be greatly reduced. On the other hand, by monitoring such signals, one can infer the state of the ionosphere, and with supporting data, associate the plasma irregularities with physical processes in the ionosphere (Spogli et al., 2009; Prikryl et al., 2011; Jin et al. 2015, 2016; De Franceschi et al., 2019; Skjæveland et al., 2021).

While receivers on the ground have a natural coverage limitation, Low Earth Orbit (LEO) satellites have opened up new opportunities for the scientific community to conduct global ionospheric research. With instruments located on board, it is possible to carry out in-situ measurements such as the electron density, energy of particles, the magnitude and direction of electric and magnetic field etc. This makes it possible to consider variations in the plasma parameters along the path of satellites. One such mission is the European Space Agency's Swarm mission. Launched to study primarily the Earth's magnetic field, it later became actively used to study space weather and ionospheric plasma (Stolle et al., 2013; Spicher et al., 2017; Jin et al., 2019; Wand et al., 2020; Spogli et al., 2021b). The Swarm mission consists of three satellites that were launched in November 2013 and have been collecting data continuously since then. This made it possible to carry out a number of studies with Swarm about space weather manifestations in the ionosphere focusing on such aspects as the electric and magnetic fields or plasma temperature, plasma structuring and irregularities (https://earth.esa.int/web/guest/missions/esa-eo-missions/swarm/activities/publications). The results from the first seven years of this mission which are related to ionospheric physics were reviewed by Wood et al. (2022).

The 3 satellites (Swarm A, Swarm B and Swarm C) constituting the Swarm satellite mission (Friis-Christensen et al., 2008) follow a quasi-Sun-synchronous near-polar orbit. The orbital altitudes of closely-separated Swarm A and C satellites are about 460 km (with separation by 1.4° in longitude). The orbit of Swarm B is at an altitude of 530 km. Thus, Swarm flies in the topside of the ionosphere, where irregularities are usually less likely to occur because plasma formations (that lead to influence the propagation of *trans*-ionospheric radio waves) such as Polar Cap Patches (PCP), the main ionospheric trough, auroral particles, Equatorial Plasma Bubbles (EPBs), and smaller irregularities that arise at the boundaries are formed in the *F* (and *E*) regions of the ionosphere (Burke et al. 2003; Roddy et al. 2010). It should be noted that in geomagnetically active conditions irregularities can be observed at the altitudes of the Swarm satellite orbits. Also, the orbital characteristics and sampling rate of the instruments fix the typical scales investigated by Swarm to values that are not suitable for ionospheric scintillations. The speed of Swarm satellites is about 7.5 km/s, which corresponds to a scale of 7.5 km (when the relative turbulence intensity is small), if in-situ electron density is sampled at a 1 Hz rate. Conversely, high-rate observations of L-band signals for the GNSS observational geometry can investigate scales that are below a few hundred meters, if the signal is recorded on the ground. Despite this, there are studies that show a relationship between observations of irregularities at the height of the Swarm flyby and scintillations on the ground (Olwendo et al., 2019; Aol et al., 2020). For example, Aol et al. (2020) presented comparison observations of ionospheric irregularities with 16-Hz Swarm electron density data, being able to investigate irregularities with a scale of about 470 m, with the Swarm satellites and L-band amplitude scintillation data from the receiver in Mbarara (low latitude) in the period from 2014 to 2018. They suggested that in-situ density fluctuations may be used to indicate the risk that ionospheric radio wave scintillations occur at that site. However, in some of their cases, ionospheric irregularities were not associated with significant scintillation, or the amplitude scintillations were seen without Swarm recording significant density variations.

In this work, we aim to demonstrate the feasibility of using Swarm data as a proxy for the scintillation activity. In previous work, Jin et al. (2020) demonstrated that the Swarm based IPIR dataset can reproduce the global climatology of ionospheric irregularities (and the resulting scintillations) that was initially summarised by Basu et al. (1988a, 1988b) based on the data from the ground-based receivers. In this study, we will take a step forward and make a direct comparison between the global Ionospheric Plasma IRregularities (IPIR) product based on Swarm measurements (Jin et al., 2022) and ground-based scintillation data. IPIR product characterises ionospheric irregularities and fluctuations and addresses the needs of the scientific community that aims to understand plasma irregularities, as well as operational users that are affected by them. From a statistical perspective, we performed validation of IPIR against ground-based measurements. We focused on the GPS Total Electron Content (TEC) and scintillation data from 23 receivers located in polar, auroral and equatorial regions since scintillation is primarily associated with equatorial regions and high latitudes and is usu-

ally weak at mid-latitudes (Basu et al., 1988a, 1988b; Basu & Groves, 2001). We show an empirical relationship that can be used to infer ionospheric impact on L-band where GNSS observations are not available (oceans, deserts, etc.). Ionospheric physics has been of particular interest in the last decade due to the increasing importance of GNSS, of which the best known is GPS. Therefore, a good understanding of ionospheric plasma irregularities and fluctuations are of both scientific and practical interest.

## 2. Approach and instruments

### 2.1. GNSS data

To conduct our study, we used 23 selected Ionospheric Scintillation Monitor Receivers (ISMRs) to cover the polar cap, cusp, auroral and equatorial regions, as these are the regions of different processes in the ionosphere. ISMRs are professional receivers dedicated to TEC and scintillation monitoring (Van Dierendonk et al., 1993; Bougard et al., 2011). They are characterised by multi-frequency capabilities, high sampling rate (50/100 Hz), low noise and stable oscillators for accurate phase measurements, and by a firmware being able to provide in quasi-real-time the phase and amplitude scintillation indices. The scintillation indices that are traditionally adopted to quantify scintillation of *trans*-ionospheric signals (Fremouw et al., 1978) are defined for phase (1) and amplitude (2) scintillation respectively as:

$$\sigma_{\varphi} = \sqrt{\langle \phi_{detr}^2 \rangle - \langle \phi_{detr} \rangle^2} \tag{1}$$

$$S_4 = \sqrt{\frac{\langle SI^2 \rangle - \langle SI \rangle^2}{\langle SI \rangle^2}} \tag{2}$$

in which $\Phi_{detr}$ is the detrended phase, $<\ldots>$ is the ensemble average, and $SI$ represents the signal intensity. These indices are based on statistical features. They are evaluated on a 1 min time window, a good compromise between the need for a large dataset and for catching rapidly evolving phenomena such as scintillations.

The detrending of the phase measurements is a very debated issue as it arises from the need to remove the effect of the satellite movement in $\sigma_{\varphi}$ determination, and the detrending scheme (including cutoff frequency) significantly affects this determination, as demonstrated by Forte (2005; 2007) and applied by Spogli et al. (2021a).

The differences in the meaning of scintillation, and the perils of using the phase scintillation index retrieved with fixed cut-off frequency are widely addressed in the literature (Forte and Radicella, 2002; Forte 2005; Beach, 2006; Mushini et al., 2012; Carrano and Rino, 2016; Wang et al., 2018; De Franceschi et al., 2019; McCaffrey and Jayachandran, 2019; Ghobadi et al., 2020; Spogli et al., 2021a; Song et al., 2021). Bearing this in mind, we decide to use the standard $\sigma_{\varphi}$ (calculated from one minute of ISMR data, detrended with a sixth-order Butterworth filter with a cut-off frequency of 0.1 Hz) as a proxy for the presence of irregularities covering the full range of scale sizes at all latitudes. This has a twofold benefit: (i) we consider irregularities of the scale-size including those detectable with Swarm satellites, (ii) the computational complexity is reduced, as we can leverage directly on the dataset provided by the ISMRs firmware and not on a customized $\sigma_{\varphi}$ which requires a reanalysis of the full raw dataset at 50 Hz. Additionally, the simultaneous use of standard $\sigma_{\varphi}$ and S4 can support the speculation about the scale-size of the irregularities involved, as enhancements of the latter are triggered only by small-scale irregularities (hundreds of meters) (Wernik et al., 2003).

The locations of ISMRs as well as their respective field of view with an elevation angle of 30° are shown in Fig. 1. Such receivers are managed by several institutions: which includes the University of Oslo, Istituto Nazionale di Geofisica e Vulcanologia (Upper atmosphere and radio propagation working group, 2020), Tromsø Geophysical Observatory and SANSA Space Science, Institute of Geology and Geophysics of the Chinese Academy of Sciences, and Peking University. The geographic coordinates, site names, type of receivers, the noise level for amplitude and phase scintillations indices together with the time intervals of the dataset are presented in Table 1. In order to construct a homogenous dataset from different receivers, among which some do not have multi-constellation capabilities (GSV4004B), we consider only data from Global Positioning System (GPS) satellites. It should be noted that the data from the Brazilian stations: Boa Vista, Belo Horizonte and Dourados operated by the EMBRACE, did not contain the measurements of the phase scintillations index ($\sigma_{\varphi}$). However, they are kept to cover the Brazilian sector, which is of particular interest as it is characterised by the presence of irregularities that are due to Equatorial Plasma Bubbles (EPB) and by the particle precipitation from the inner radiation belt down to the atmosphere due to the South Atlantic Magnetic Anomaly (Abdu et al., 2005; Spogli et al., 2013; Whittaker et al., 2013).

For each receiver, we used data with the satellite elevation angle above 30° to reduce the multipath effects that may mimic scintillation events. Since in this work we want to test the possibility of using data from the Swarm satellite flyby height as a marker for scintillations observed on receivers on the ground, we needed to level the values of the scintillation indices responsible for noise interference or minor scintillations. To calculate the noise level of the scintillation indices, we performed statistical analysis for each receiver. To do this, for the entire available dataset for each receiver, a histogram of the distribution of values was plotted. We present the distributions of amplitude and phase scintillation index values in Fig. 2 as an example for polar and low-latitude stations, and determine the level (with a density threshold of 10 % of the maximum value and using the corresponding $\sigma_{\varphi}$ or S4 value from the right side of the distribution), below which the measurements were considered to be noise.

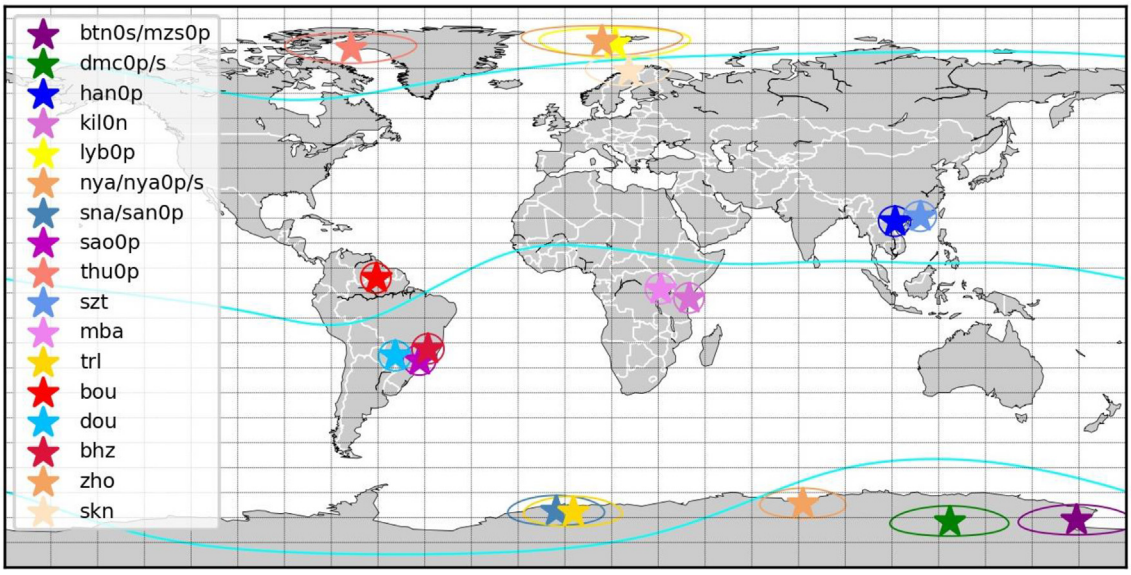


Fig. 1. Locations of ISMRs depicted by stars surrounded by thin ellipses showing their respective field of view above a 30° elevation angle at a height of 350 km. The blue lines show 70°N, 0° and 70°S geomagnetic parallels.

Table 1
Site names, stations, locations, and type of ISMRs, together with the noise level for phase and amplitude scintillation indices and used time intervals for the dataset.

| Site name | Station | Lat., deg | Long., deg | Receiver type | $\sigma_{\varphi}$_nl, rad | S4_nl | Available dataset |
|---|---|---|---|---|---|---|---|
| nya | Ny-Ålesund | 78.92 | 11.93 | NovAtel GSV 4004B | 0.07 | 0.06 | 2014/07/16–2022/06/21 |
| nya0p | Ny-Ålesund | 78.90 | 11.90 | Septentrio PolaRxS/PolaRx5s | 0.04 | 0.04 | 2015/11/09–2020/12/04 |
| nya0s | Ny-Ålesund | 78.90 | 11.90 | NovAtel GSV 4004B | 0.07 | 0.06 | 2014/07/16–2020/09/17 |
| lyb0p | Longyearbyen | 78.20 | 16.00 | Septentrio PolaRx5S | 0.05 | 0.06 | 2019/01/13–2021/10/31 |
| lyb0s | Longyearbyen | 78.20 | 16.00 | NovAtel GSV 4004B | 0.07 | 0.06 | 2015/03/10-2017/10/06 |
| thu0p | Thule | 76.51 | −68.74 | Septentrio PolaRx5S | 0.05 | 0.035 | 2021/04/29–2021/10/31 |
| skn | Skibotn | 69.35 | 20.36 | NovAtel GSV 4004B | 0.06 | 0.08 | 2014/09/01–2022/05/22 |
| szt | ShenZhen | 22.59 | 113.97 | NovAtel GSV 4004B | 0.06 | 0.06 | 2014/09/09–2014/12/28 |
| han0p | Hanoi | 21.00 | 105.84 | Septentrio PolaRxS | 0.04 | 0.02 | 2020/09/30–2021/10/31 |
| bou | Boa Vista | 2.83 | −60.69 | NovAtel GSV 4004B | – | 0.09 | 2015; 2019 |
| mba | Mbarara | −0.60 | 30.74 | NovAtel GSV 4004B | 0.07 | 0.08 | 2015; 2019 |
| kil0n | Kilifi | −3.60 | 39.80 | NovAtel GPStation-6 | 0.11 | 0.07 | 2019/05/14–2021/10/31 |
| bhz | Belo Horizonte | −19.87 | −43.96 | NovAtel GSV 4004B | – | 0.08 | 2015; 2019 |
| dou | Dourados | −22.11 | −54.55 | NovAtel GSV 4004B | – | 0.1 | 2015 |
| sao0p | São Paulo | −23.50 | −46.70 | Septentrio PolaRxS | 0.04 | 0.05 | 2017/05/31–2021/10/31 |
| zho | Zhongshan | −69.38 | 76.38 | NovAtel GSV 4004B | 0.07 | 0.08 | 2014/07/15–2014/12/31 |
| san0p | SANAE IV | −71.70 | −2.80 | Septentrio PolaRxS | 0.04 | 0.05 | 2015/12/27–2021/10/31 |
| sna | SANAE IV | −71.67 | −2.84 | NovAtel GSV 4004B | 0.07 | 0.065 | 2018/01/01–2020/12/31 |
| trl | Troll | −72.00 | 2.52 | NovAtel GPStation-6 | 0.13 | 0.08 | 2018; 2019; 2020; 2021 |
| btn0s | Mario Zucchelli | −74.70 | 164.11 | NovAtel GSV 4004B | 0.07 | 0.06 | 2014/07/16–2019/01/03 |
| mzs0p | Mario Zucchelli | −74.70 | 164.11 | Septentrio PolaRxS | 0.05 | 0.06 | 2016/11/29–2021/10/29 |
| dmc0p | Concordia | −75.10 | 123.40 | Septentrio PolaRx5s | 0.04 | 0.05 | 2017/01/29–2021/10/29 |
| dmc0s | Concordia | −75.10 | 123.40 | NovAtel GSV 4004B | 0.07 | 0.06 | 2014/08/16–2021/10/29 |

### 2.2. Swarm data

In-situ measurements of plasma irregularities and fluctuations can be successfully carried out by the Swarm satellites with their complementary datasets, i.e. the plasma density from the electric field instrument, the GPS data from the onboard GPS receiver, and the magnetic data from the vector field magnetometer, as well as Level-2 Swarm data products (https://swarm-diss.eo.esa.int/#swarm%2FLevel2daily%2FLatest_baselines). The IPIR product is based on Swarm data and combines Level 1b data products for Swarm: plasma density, magnetic field, and level 1 and level 2 data from the onboard GPS receivers. The IPIR product characterises the plasma density fluctuations and irregularities encountered by Swarm in terms of their amplitudes, gradients and spatial scales and assigns them to geomagnetic regions and consequently to predominant plasma processes. The IPIR product also

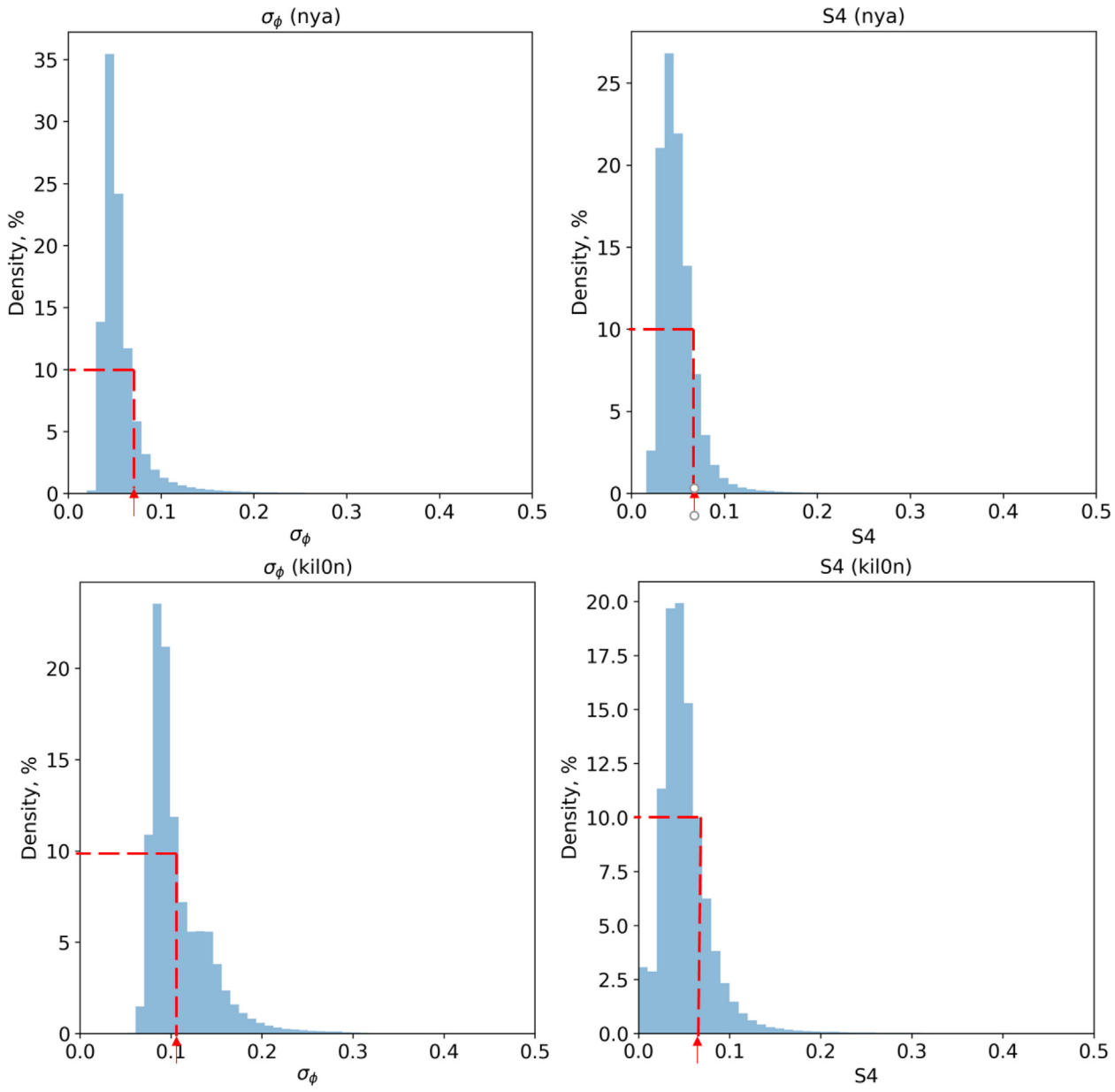


Fig. 2. Histogram of distribution of $\sigma_{\varphi}$ (left) and S4 (right) from the receivers at Ny-Ålesund (top) and Kilifi (bottom). The red dashed line shows the threshold of 10 %, which we used as the noise boundary. Thresholds for $\sigma_{\varphi}$ and S4 are 0.07 rad and 0.06 for Ny-Ålesund and 0.11 rad and 0.07 for Kilifi, respectively.

provides an indication, in the form of a numerical value index (IPIR index, $IPIR_{ix}$), on their severity for the integrity of *trans*-ionospheric radio signals and hence, the accuracy of GNSS precise positioning. The IPIR product relates the fluctuations to the ionospheric current system and variations in the magnetic field, in order to relate these structures to dynamic phenomena in the ionosphere. Finally, it combines data from the GPS receivers, where TEC and Rate of Change of TEC (ROT) provide information on the extent of the structures in the direction of the GPS satellites (more details about the IPIR product can be found in Jin et al., 2022).

### 2.3. GNSS-Swarm conjunction points

In order to compare the IPIR product with ground-based GPS data, we need to find time intervals when the Swarm satellites passed over the field of view of the ground-based GPS receivers. To give a sense of the conjunction geometry, we show in Fig. 3 an example of the conjunction between the Swarm and GPS satellites. Here we used only those times for which the Swarm satellite flew over the ground-based receiver's field of view. To compare the characteristics of electron density fluctuations from Swarm with ground-based scintillation data, we performed

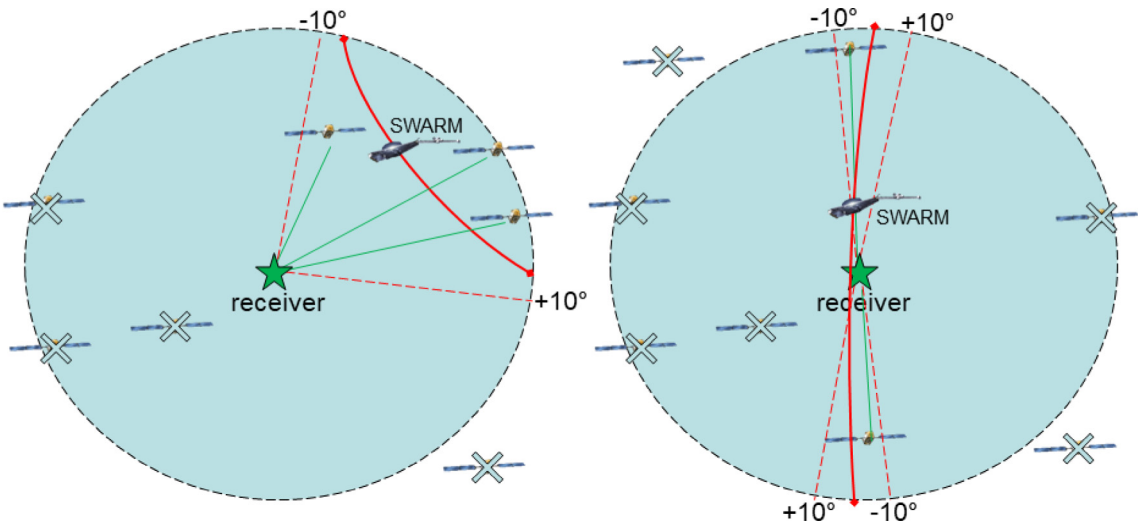


Fig. 3. Geometry for finding conjunction points. The blue fill shows the receiver's field of view at 30° elevation angle and assuming ionospheric pierce points (IPPs) at 350 km, the red line shows the locus of the Swarm satellite, the red dashed line shows the azimuth sector in which the GPS satellites were considered (green lines). Crossed out are those satellites of which data were not used in the study. A case where the path of the Swarm satellite is near the edge of the 30° elevation cone centered on the ground-based receiver show in the left. A case where the Swarm satellite is almost overhead of the ground-based receiver shown in the right.

an azimuthal selection of the GPS data according to Swarm satellite overpass (azimuth ± 10°). We used only those GPS satellites that emerged in the azimuth sector. After this selection of data, we can consider the measured parameters for the same area and carry out the analysis.

The two data sets have different temporal resolutions (Swarm 1-s and GPS 60-s). To enable these datasets to be compared the Swarm measurements are taken 30 s before and after the available GPS measurement time. For example, for a GPS satellite that passed over in the azimuth sector for two minutes from 15:36:00 UT to 15:38:00 UT Swarm data was taken for a time period from 15:35:30 UT to 15:38:30 UT. The median, mean, maximum and standard deviation values for both the Swarm and ground-based parameters are also taken for this interval (for each PRN satellite). From the receiver on the ground, we have the behaviour of Vertical and Slant TEC (VTEC and STEC), the ROT and Rate Of Change of TEC Index (ROTI), amplitude (S4) and phase scintillation ($\sigma_{\varphi}$) indices. The analysis does not take into account values below the threshold set for each station and receiver (see Table 1). As TEC measurements are affected by various sources of errors, such as inter-frequency biases, multipath, phase ambiguity and cycle slips (Ciraolo et al., 2007; Cesaroni et al., 2021), a TEC calibration procedure is usually needed. In this analysis, the slant TEC data from ground-based GNSS receivers was calibrated using the software WinTEC-P (Carrano et al., 2009) and projected to the vertical at 350 km by applying a mapping function (Mannucci et al., 1998). From the receiver onboard the Swarm satellites, we have information about the VTEC behaviour on the ray-path between Swarm and the GNSS satellite, ROT from all available GPS satellites above 30°, and ROTI. ROTI calculations were based on the vertical TEC (Jin et al., 2022). The procedure to calibrate and project to the vertical of the TEC values from Swarm is described in the TEC product description (https://earth.esa.int/eogateway/documents/20142/37627/swarm-level-2-tec-product-description.pdf/8fe7fa04-6b4f-86a7-5e4c-99b-b280ccc7e), and relies also on earlier work on CHAMP satellite data by Noja et al. (2013). From the Langmuir probe at the height of the Swarm satellite, we can get data such as plasma density (*Ne*), Rate Of change of Density (ROD), Rate Of change of Density Index (RODI), gradients and amplitude of *Ne*. All these parameters from Swarm are conveniently organised in the IPIR dataset (Jin et al., 2022). This product is freely available at the ESA Swarm dissemination servers (https://swarm-diss.eo.esa.int/#swarm/Level2daily/Latest_baselines/IPD/IRR) and can be found as IPDxIRR_2F (where, x = A, B or C, defines the Swarm satellite). The IPIR dataset consists of 29 entries including parameters for characterising plasma structuring.

## 3. Results of validation

### 3.1. Polar cap and cusp stations

To derive the long-term statistics of the conjunction observation, we used data from 11 receivers located in the polar cap and cusp area of both hemispheres (site names are nya, nya0p, nya0s, thu0p, lyb0p, lyb0s, zho, dmc0s, dmc0p, btn0s, mzs0p). Fig. 4 shows the scatter plots of VTEC from considered receivers versus VTEC and electron density from Swarm A. We chose to use scatter plots to present the degree of correlation between two independent variables. In all obtained results (Figs. 4-10) data from Swarm was plotted along the horizontal axis and data from

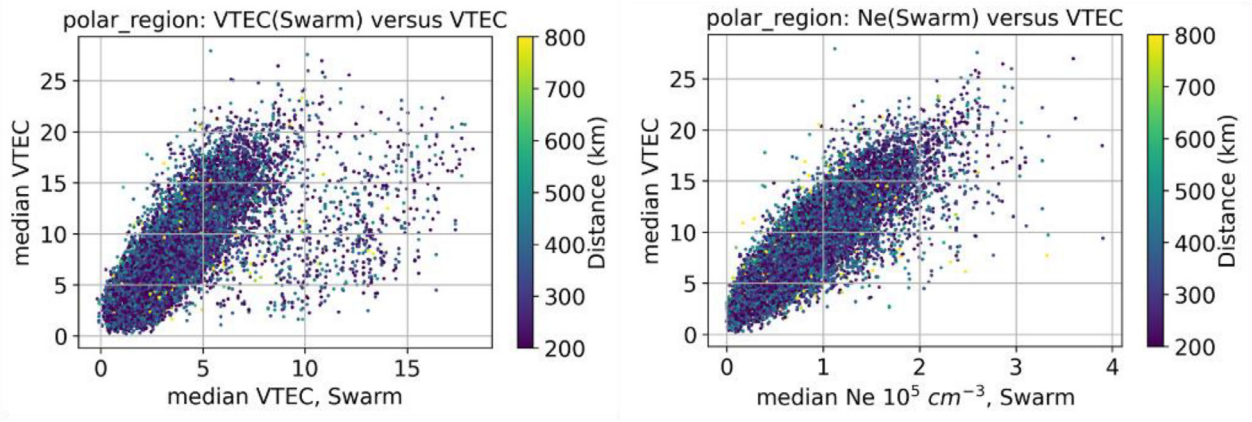


Fig. 4. Scatter plots of median VTEC and electron density from Swarm A versus median VTEC from ground-based GPS receivers in the polar region. Each point represents one conjunction. The colour coding shows the distance between Swarm A and the IPPs of the ray paths from the GPS satellites.

receivers along the Y-axis. This representation was chosen because we want to reflect on the relationship between Swarm and ground-based receiver measurements to show the possibility of using the Swarm data in areas where data from ground-based receivers are not available. We used data only when the Swarm satellite passed over the field of view for more than 60 s. In the scatter plot, one point represents one conjunction of the ground-based receiver and Swarm satellite, in the same manner, as it is explained in section 2.3. For observations related to each GPS satellite, the distance between the ionospheric pierce point of the ray path to the GPS satellite at a height of 350 km and the Swarm satellite was calculated and colour-coded in Figs. 4-10. It is clear that both density and VTEC measured from space show a good correlation with the VTEC observation from the ground (Fig. 4). We can see on the plot of VTEC data from ground-based GPS receiver vs Swarm that for some of the data the Swarm VTEC is higher by about 10 TECU units than the corresponding values for the receiver on the ground. This can be explained by the fact that these points were mainly obtained during a high level of solar activity in 2014–2015. Also, we found that for a range of full calendar days there is an unexplained calibration offset between relatively closely-separated Swarm A versus Swarm C in VTEC data, where those were matching very well on the surrounding days (e.g., 17 March 2015 where the difference of $\sim$ 10 TECU between those two satellites remained during the whole day as shown in Figure SM0 in the Supplementary Materials). The data from the Langmuir probe does not show a similar offset as the receiver onboard Swarm. Since the processed data set contains about 8 years of data the main part of the data was obtained during a period of low solar activity (see Table 1), so the trend in the left part of the figure is more pronounced. This correlation with solar activity was well-demonstrated for the polar caps of both hemispheres by Jin et al. (2019). Comparing the values of the in-situ electron density from the Swarm satellite with the VTEC values of the upper part of the ionosphere, we do not see a similar trend of high values suggesting an occasional calibration issue with Swarm VTEC during high geomagnetic activity.

Fig. 5 shows a comparison between ground-based measurements of the phase scintillation $\sigma_\varphi$ (Fig. 5a) and amplitude S4 (Fig. 5b) indices and four selected parameters from Swarm A, namely: RODI, ROTI, the standard deviation of the electron density (std(Ne)) during the time interval when Swarm passes the field of view of the ground-based receivers and the density gradient at 100 km scale ($\nabla$Ne). The irregularity parameters from Swarm are correlated with the ground-based phase scintillation strength, that is when RODI (ROTI, std(Ne), $\nabla$Ne) increases, we see increases in $\sigma_\varphi$ and S4 as well. However, the relationship is not linear. But it can be noted that for the lower part of the range of values there is a linear relationship that is observed both in the $\sigma_\varphi$ plots and in the S4 plots. Such local linear dependencies are associated with scintillation events. However, the amplitude scintillation index is weakly correlated (shows a positive correlation) with the Swarm-derived irregularity parameters. The main reason for this is that S4 is related to irregularities at scales of hundreds of metres, corresponding to a Fresnel scale for GNSS signals received on the ground (Yeh & Liu, 1982), while Swarm allows for detecting density gradients down to several km scales. Nevertheless, for large fluctuations in density observed by Swarm, we expect smaller scale fluctuations to be present as well as a result of turbulence and instability cascading (when the conditions for cascading are favourable), and thus we expect the linear relationship between the two quantities, especially at the edges of polar cap patches (Coker et al., 2004; Jin et al., 2017; Jayachandran et al., 2017).

### 3.2. Auroral stations

The auroral region (Figs. 6-7) has the least coverage of all regions and is represented by only 4 stations (site names are skn, trl, sna, san0p). Despite this, the following conclusions can be drawn. It is evident that, again, for this region, there is a positive correlation between VTEC measurement on the ground, median VTEC and median *Ne*, as measured

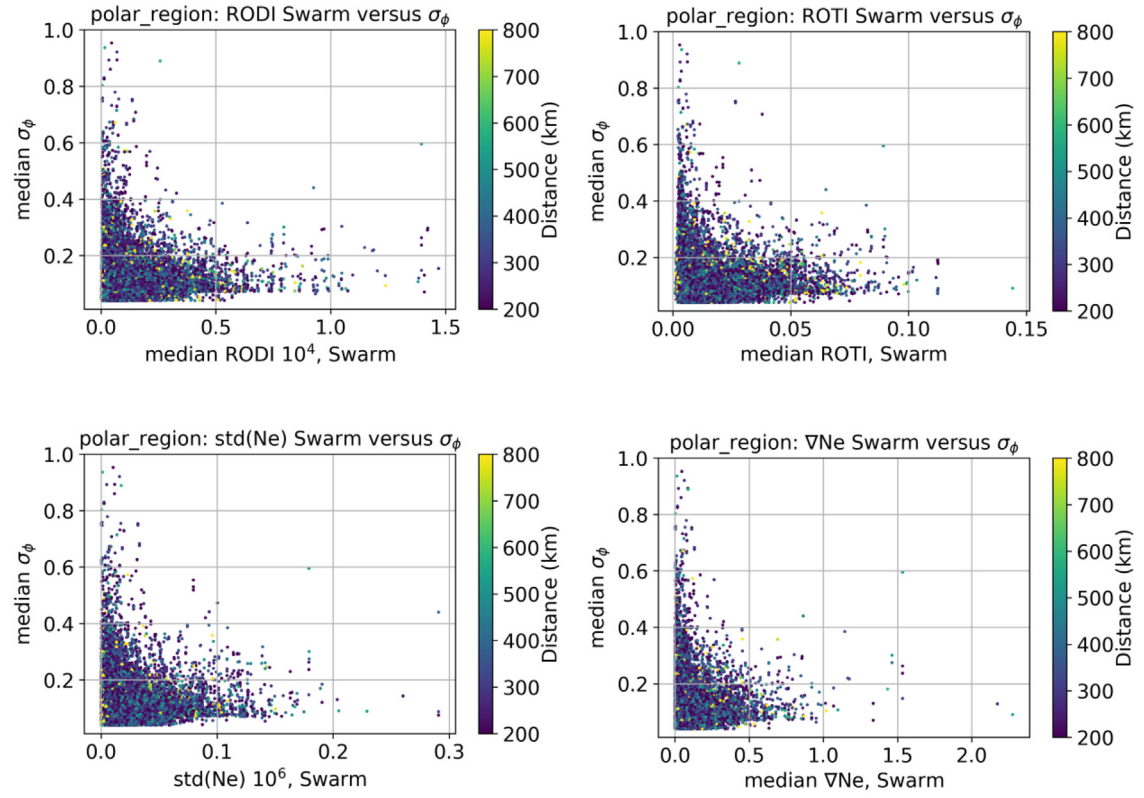


a

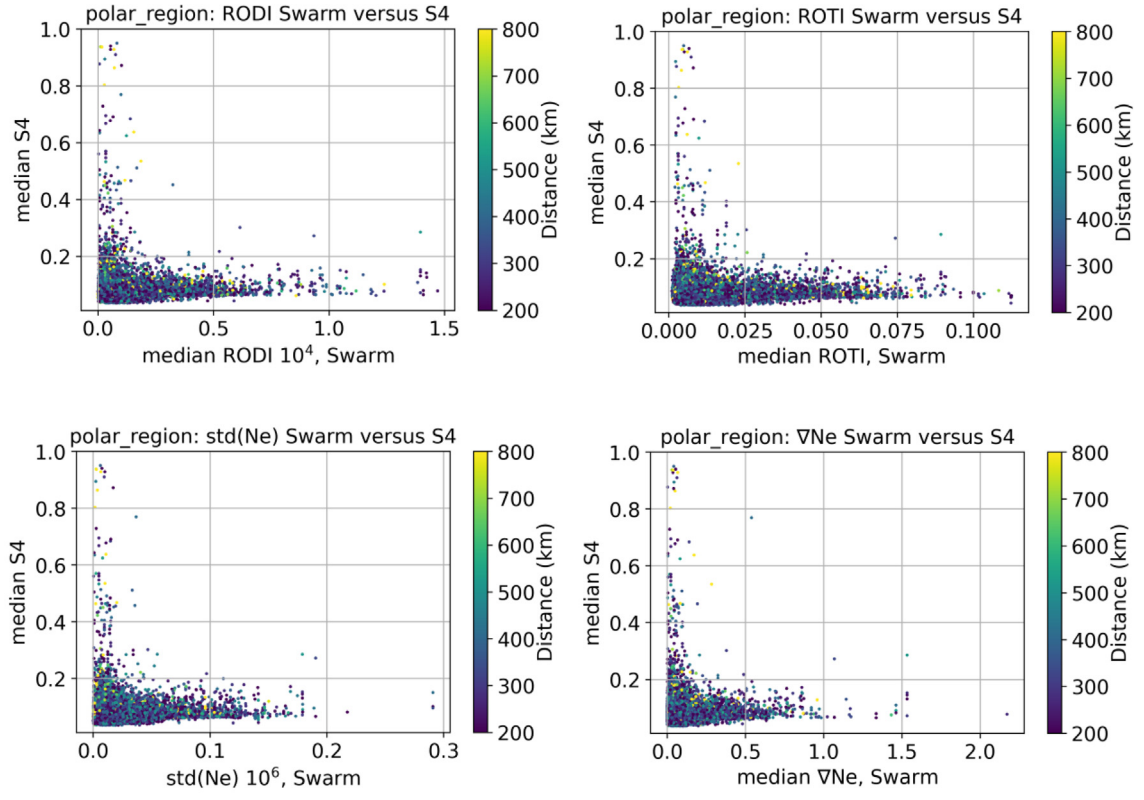


b

Fig. 5. Scatter plots of the median values of phase (a) and amplitude (b) scintillation index from ground-based receivers located in the polar regions versus selected parameters from Swarm A: median RODI, ROTI, std(Ne), and the density gradient at 100 km scale (∇Ne). The colour coding shows the distance between Swarm and the IPPs of the ray paths from the GPS satellites.

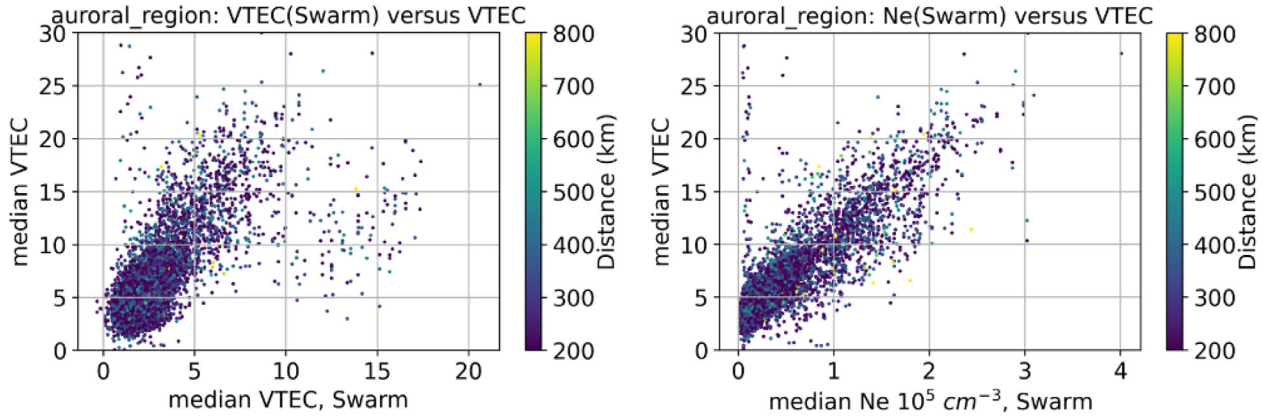


Fig. 6. Same as Fig. 4 but for the auroral region.

by Swarm (Fig. 6). The stronger correlation between *Ne* and ground-based TEC measurements are due to the fact that the electron density decreases with altitude, and thus the local plasma density is more likely representative of the VTEC measured on the ground. We see a similar additional linear trend in Swarm's VTEC plot (not as pronounced due to the small number of available data points), which is also related to the uneven distribution of data with respect to the level of solar activity (the combined dataset is dominated by data for low solar activity, see Figure SM1).

There is a non-trivial relationship between median phase and amplitude scintillation index and parameters measured by Swarm (Fig. 7). The presence of the two-level clustering of $\sigma_\varphi$ (around 0.06 and 0.13 rad) is apparently associated with the use of individual thresholds for each receiver (see numbers in Table 1 $\sigma_{\varphi\_nl}$ for stations SKN and TRL). It is also worth noting rather high values of the phase scintillation index (several points on the top side of the figures), which are not related to variations in the parameters measured by Swarm. This is due to very dynamic ionospheric conditions in the auroral region, where the median scintillation index may not be representative of the actual conditions encountered by Swarm. In the polar cap region, plasma irregularities can stretch along magnetic field lines and thus manifest themselves in the *F* region (close to the orbital altitude of the Swarm satellite, see Rodger et al., 1994; Lorentzen et al., 2004). However, in the auroral region, the altitude of the emergence of irregularities can be related to currents associated with (auroral) precipitation of particles in the *E* region of the ionosphere, which is much lower than the orbital altitude of the Swarm satellite. Therefore, Swarm observations may not reflect strong GPS scintillations observed from the ground at auroral stations.

### 3.3. Low-latitude stations

We used 8 low-latitude stations located near the equatorial anomaly (see Fig. 1, site names are sao0p, kil0n, dou, bhz, mba, bov, han0p, szt), where the receiver is affected by scintillation due to the small-scale irregularities embedded in the EPBs (Li et al., 2021). As stations are at low latitudes, there are fewer conjunction points than for the high-latitude stations. In addition, data covers mainly 2015 and 2019–2021 (see Table 1). Fig. 8 shows the scatter plot of VTEC from the ground-based GPS receivers versus *Ne* as well as VTEC measured onboard Swarm. We see here that the linear dependence is no longer so pronounced as discussed in sections 3.1 and 3.2. There is an increase in scatter as the values increase. With an increase in the parameters measured by Swarm, the values of VTEC on the ground also increase (positive correlation).

We also compared the four selected irregularity parameters from Swarm with the ground-based phase and amplitude scintillation indices in Fig. 9 which show a weak correlation between the ground-based irregularity parameters and the space-based ones. There were no observations of $\sigma_\varphi$ from three stations in this region. It can be seen that S4 achieves a higher correlation with measurements from Swarm compared to $\sigma_\varphi$. In S4 plots, there are more events associated with irregularities in comparison with the polar region (separated linear relations) which may be associated with plasma bubbles. It is worth noting that it was shown by Smith and Heelis (2017) that plasma bubbles can also be observed at altitudes corresponding to the Swarm orbital altitudes. The maximal values of parameters plotted on the X-axes also increased significantly, especially for std (Ne) and ∇Ne compared to Figs. 5 and 7.

## 4. Scale validation for the IPIR index

As described in (Jin et al., 2022), the IPIR index provides information on the level of ionospheric fluctuations based on their temporal variations and amplitude. $\mathrm{IPIR_{ix}}$ aims to capture both the amplitude and degree of structuring of plasma and is a product of the two estimates RODI in 10 s and the standard deviation of delta *Ne* in 10 s (i.e., of $\Delta n_{e10s}$):

$$\mathrm{IPIR}_{ix} = \mathrm{RODI10}s \cdot A(n_e)_{10s} \quad (3)$$

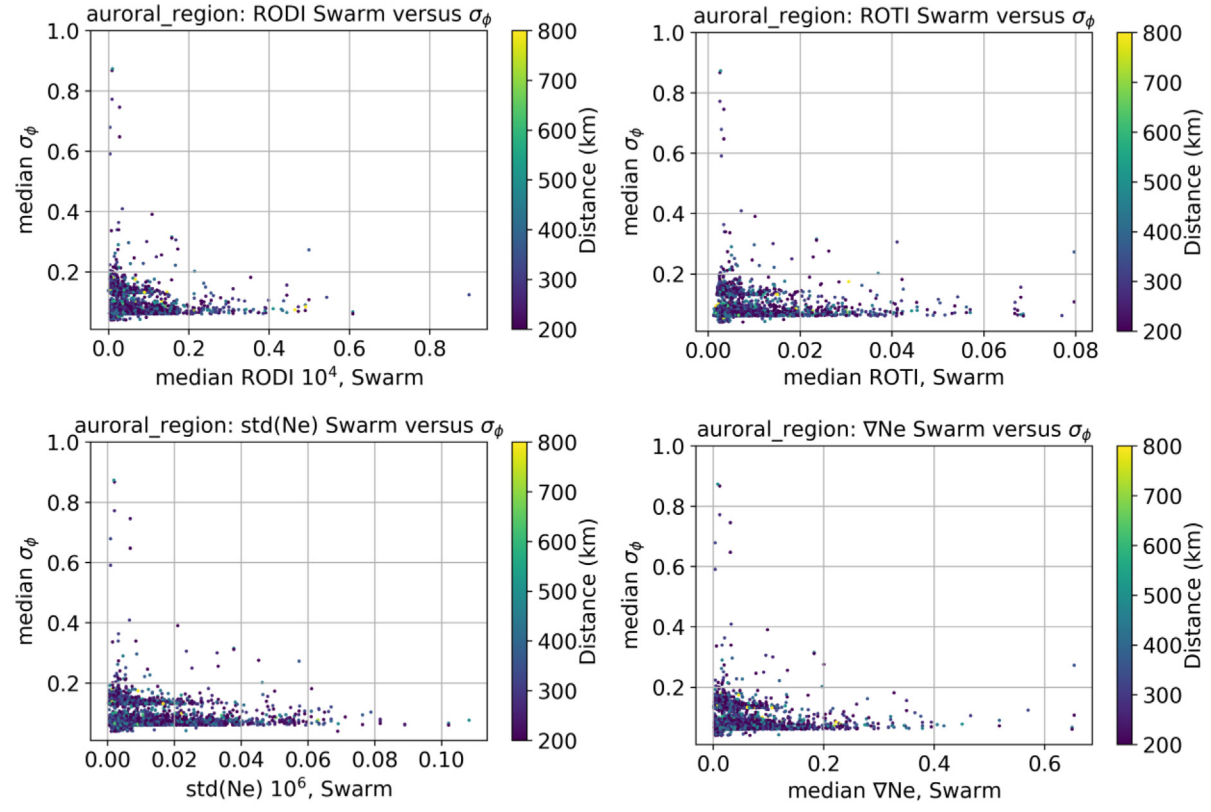


a

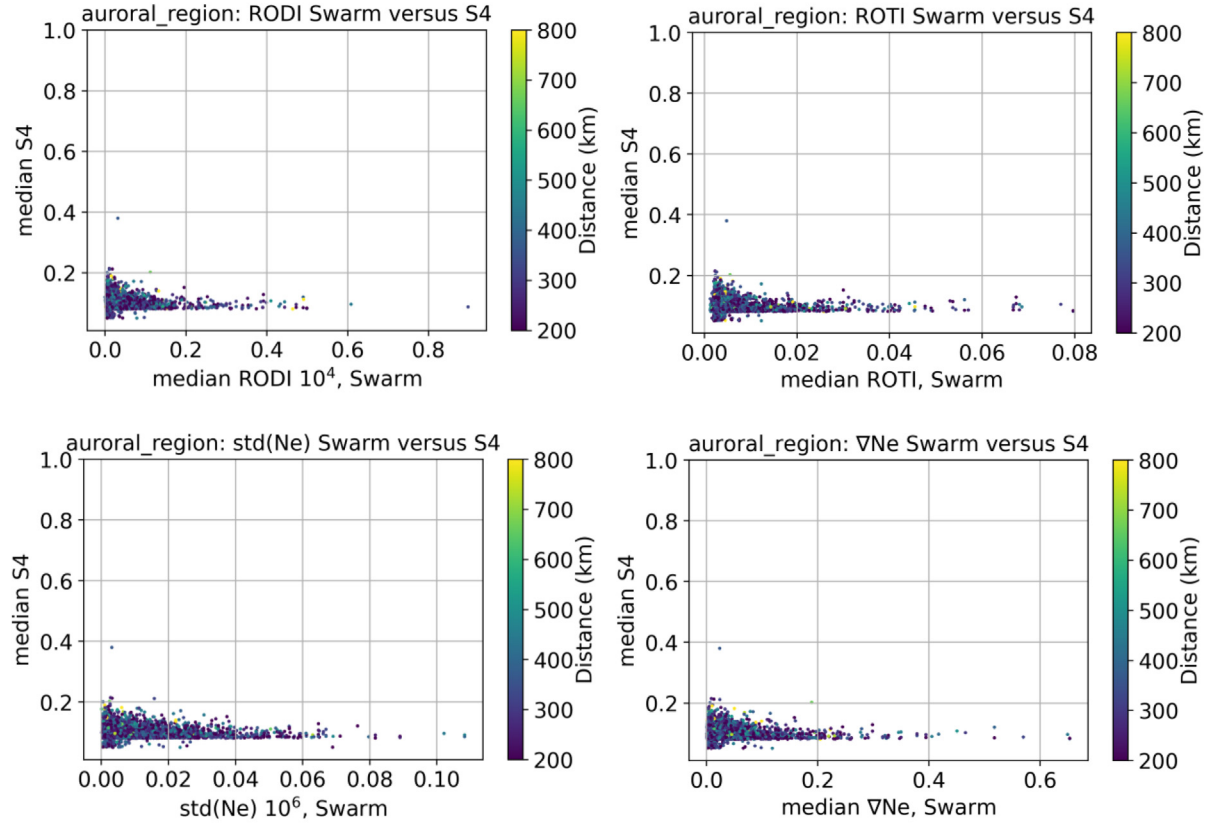


b

Fig. 7. Same as Fig. 5 but for the auroral region.

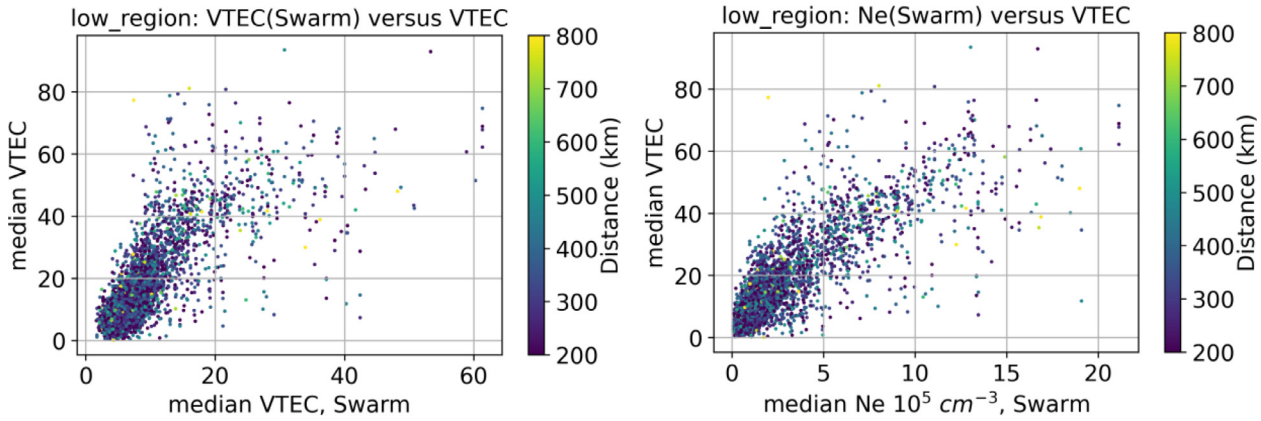


Fig. 8. Same as Fig. 4 but for a low-latitude region.

where $A(n_e)_{10s}$ is the standard deviation of $\Delta n_{e10s}$ in a running window of 10 s:

$$A(n_e)_{10s}(t) = \sqrt{\frac{1}{N-1}\sum_{t_{i=t-\Delta t/2}}^{t_{i=t+\Delta t/2}} \left|\Delta n_{e10s}(t_i) - \bar{\Delta n}_{e10s}\right|^2} \quad (4)$$

where $\bar{\Delta n}_{e10s}$ is the mean value of $\Delta n_{e10s}(t_i)$ in this time interval:

$$\bar{\Delta n}_{e10s} = \frac{1}{N}\sum_{t_{i=t-\Delta t/2}}^{t_{i=t+\Delta t/2}} \Delta n_{e10s}(t_i) \quad (5)$$

The IPIR index is thus a proxy of a local disturbance of the ionosphere along ca. 75 km of the orbit, with resolving scales down to 3.5–7 km.

In order to check and validate the scale of the IPIR index that would also reflect the impact of the irregularities on *trans*-ionospheric radio signals, we used the ground-based scintillation data. As noted in the previous section, there is no simple relation between the scintillation indices measured by ground-based GPS receivers along the ray path from GPS satellite to the ground and the plasma density irregularities that were measured in-situ by Swarm.

To relate the IPIR index to conventional ionospheric scintillation indices, we decided to use both scintillation indices from GPS receivers and compare them with the values of the IPIR index for the three regions under consideration (Fig. 10). While there is no clear linear relationship between the median of $\sigma_\varphi$ and $IPIR_{ix}$, or between the median of S4 and $IPIR_{ix}$, we do observe that both $\sigma_\varphi$ and S4 increase with increasing $IPIR_{ix}$ (the exception is the graph of S4 versus $IPIR_{ix}$ in the auroral region). It should be noted that when considering a separately selected station, rather than the overall statistics, a positive correlation is more pronounced (see Figure SM2) even in the auroral region (especially for phase scintillation index). For the low-latitude region, the range of the IPIR index was $10^3$-$10^6$ $cm^{-3}s^{-1}cm^{-3}$, and there were only a few points with a high level of phase scintillation. Larger $IPIR_{ix}$ also relates to increasing the minimal observed scintillation levels. The best statistics are shown for the polar region due to a larger dataset, while the low-latitude region is mainly described by the dataset for the period of low solar activity (see Figures SM2 and SM1). In the auroral region, there were only 4 stations considered, with coverage mostly from 2018 to 2021 (years with the low solar activity level). Here the two-level clustering of $\sigma_\varphi$ can be explained by the used threshold at four selected receivers (see Table 1 with $\sigma_{\varphi\_nl}$ at Troll 0.13 rad and 0.06 rad at Skibotn). Despite the poor statistics of this data, we still observe an increase in values of $\sigma_\varphi$ with an increase of $IPIR_{ix}$ (see Figure SM2). Thus, increased levels of $IPIR_{ix}$ may indicate an increased probability of getting GNSS scintillation events, in terms of large $\sigma_\varphi$ values. For $IPIR_{ix}$ values lower than $10^5$ $cm^{-3}s^{-1}cm^{-3}$ there is a low or very low probability of phase scintillation. The $\sigma_\varphi$ levels exceed the noise levels for numerical values of $IPIR_{ix}$ in the range $10^5$-$10^7$ $cm^{-3}s^{-1}cm^{-3}$, which we refer to as a medium probability of phase scintillation. However, for values of $IPIR_{ix} > 10^8$ $cm^{-3}s^{-1}cm^{-3}$ there was almost no very weak scintillation observed, while the mean level of phase scintillation increases and severe scintillation was more likely to be present. While for the low-latitude region, a limited number of data points for phase scintillation makes it difficult to draw firm conclusions, this region still shows a weak trend of stronger scintillation with increasing $IPIR_{ix}$.

It is worth noting that similar graphs plotted by region for the average, maximum values and standard deviation (presented in Supplementary Materials as Figures SM3-5, respectively) retain the observed relation between Swarm observations and observations by ground-based receivers. It can be noted that the mean values are slightly larger than the medians, and the spread in the mean values is larger than for the median values. This results in the graph of the mean values appearing to be shifted to the right and having a larger spread of values. The spread is also more pronounced for the maximum value graphs.

## 5. Discussion and conclusions

We followed up on previous study Jin et al. (2020), which showed that the Swarm satellite data reproduced

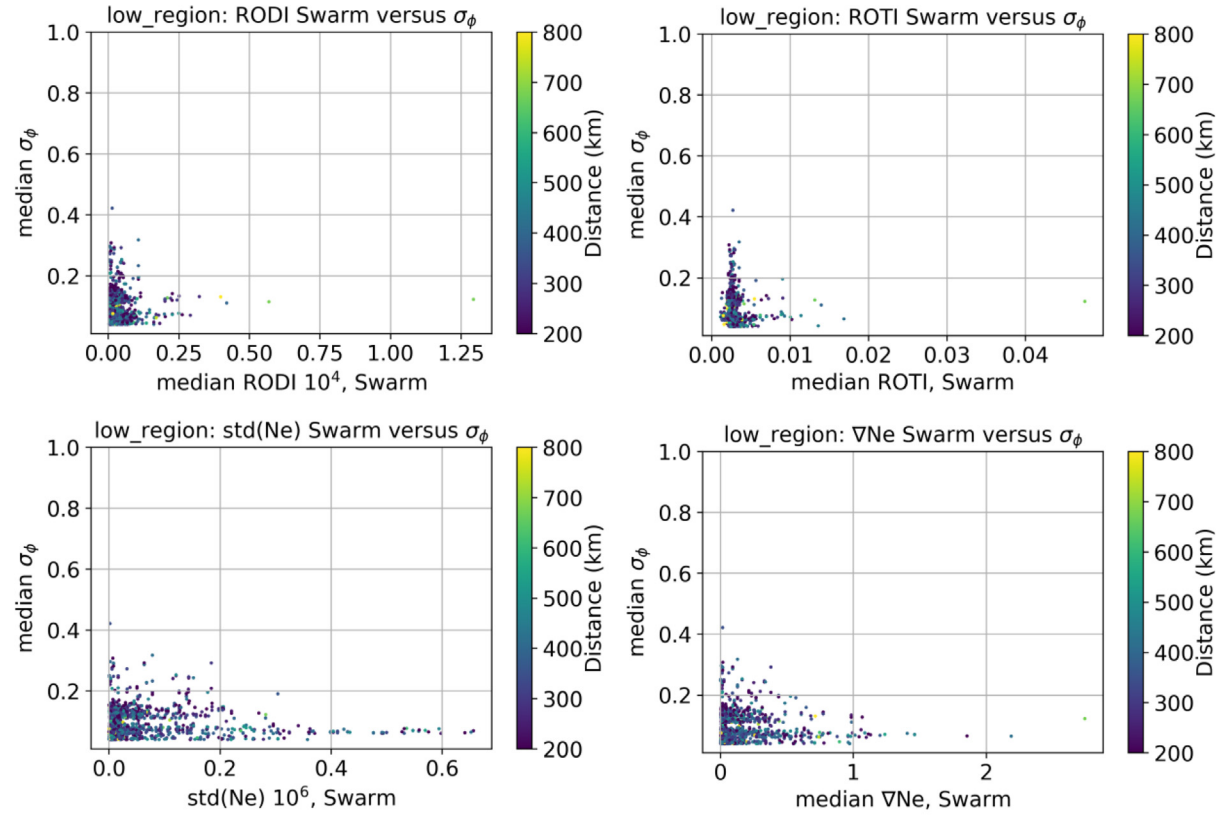


a

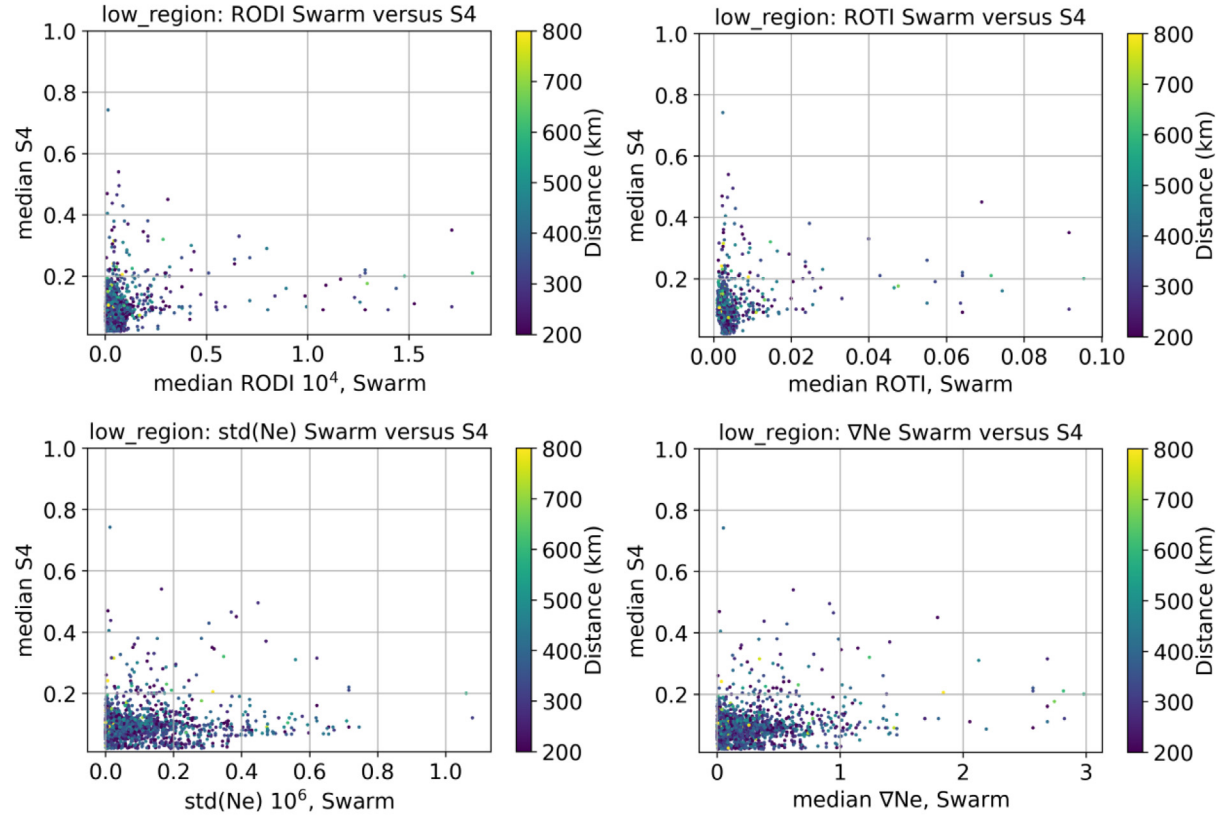


b

Fig. 9. Same as Fig. 5 but for the low-latitude (equatorial) region.

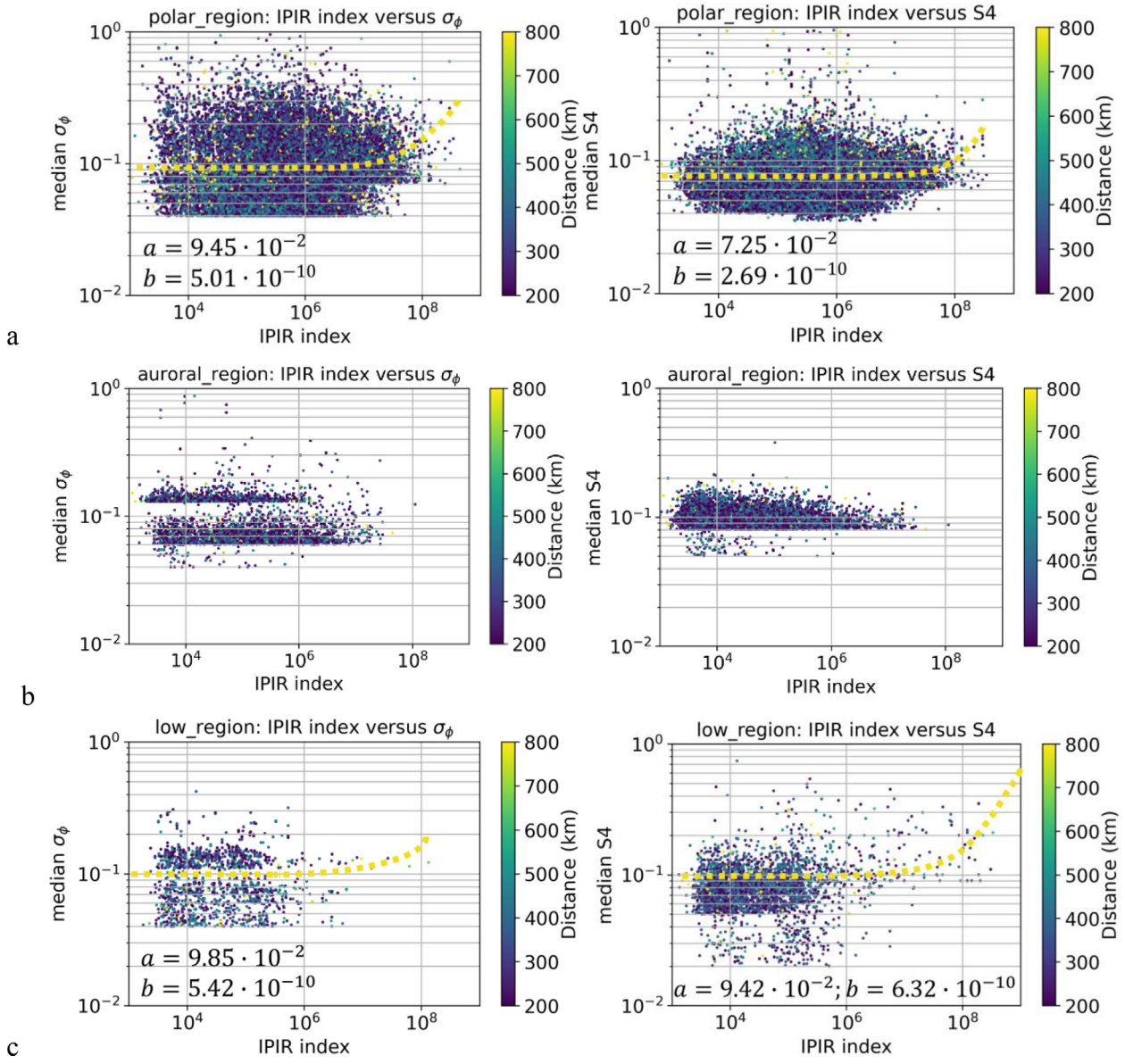


Fig. 10. Median phase ($\sigma_\varphi$, left column) and amplitude (S4, right column) scintillation indices from receivers at polar (a), auroral (b), and low (c) latitude regions versus the IPIR index. The axes are logarithmic. The colour coding shows the distance between Swarm A and the IPPs of the ray paths from GPS satellites. The yellow dotted lines represent a linear regression model fit in form $y = a + bx$, where $a$ is the intercept term, $b$ is slope ($b > 0$ show positive correlation). The $a$ and $b$ values are reported directly on the corresponding plots.

the climatology of irregularities that were generalized by Basu et al. (1988a, 1988b) based on ground-based receivers data. In the present study, we directly test how these two datasets are correlated. We compared the data from 23 ground-based GPS scintillation receivers (see Fig. 1 and Table 1) with the Swarm data during the Swarm overpass in each receiver's field of view. The studies were carried out separately for three geomagnetic regions: low, auroral and polar latitudes. This was done by considering that different plasma processes could happen in these ionospheric regions and different ionospheric phenomena cause irregularities in ionospheric electron density in the respective areas. Polar cap patches and auroral particle precipitation dominate in the polar ionosphere, while at low latitudes the influence of the equatorial anomaly and plasma bubbles prevails. All these processes lead to the formation of irregularities of various scales, which in turn affect the passage of *trans*-ionospheric signals.

By using the data only from the GPS satellites that were in the azimuth sector of the Swarm satellite passage (see Fig. 3) and presenting the results using colour-coding for the distance between Swarm satellites and the IPPs of the ray paths to the GPS satellites (where most conjunction points are separated by distances between 100 and 500 km, see Figure SM6), allows us to assume that both datasets belong to one area. We obtained a strong positive correlation between the median VTEC measured by the ground-based ISMRs at all considered regions and the fol-

lowing parameters measured by the Swarm satellites: the median values of VTEC and electron density *Ne* (Figs. 4, 6, and 8). A positive correlation was also present between the two VTEC measurements (on board and from the ground). However, there was an insignificant (to the total volume of points) additional distribution with larger VTEC values from the receiver on board the Swarm than measured on the ground. One possible explanation for this anomaly is that for a range of full calendar days an unexplained calibration offset was found between relatively closely-separated Swarm A and Swarm C in VTEC data which were not observed in the Langmuir probe data (see Figure SM0). An additional check of the data with Swarm C also showed the presence of this distribution, though not so pronounced (Figure SM7). A better linear relationship was obtained between the VTEC measured by ground receivers and the electron density measured by Swarm. This is because VTEC measurements from the ground include the electron density values below and up to the Swarm orbit, while VTEC measured by Swarm only accounts for electron densities above the satellites. It can also be noted that the topside VTEC (on the ray path between the Swarm and the GPS satellites) is more sensitive to changes in the level of solar activity. As it was shown by Yasyukevich et al. (2019), for data at a typical mid-latitude point over the time period 2010–2013, there is a significant level of correlation between Total and Plasmasphere Electron Content (TEC and PEC) and indices of solar activity (UV, F10.7). At daytime the level of TEC and PEC correlation with solar activity is significant (with a maximum value of 0.75 for TEC), and at night time it is significantly lower (with the highest value for PEC 0.46). While the correlation with geomagnetic activity indices (AE and *SYM*-H) is insignificant.

The relationship between scintillation indices measured with the ground receivers and parameters derived from the Swarm measurements is nonlinear, which is as expected (Figs. 5, 7, and 9). Scintillations are the effect of scattering and diffraction of waves in the irregular medium (Yeh and Liu, 1982), and in the case of the amplitude scintillations, these irregularities are in the order of hundreds of metres for L-band frequencies (Forte and Radicella, 2002; Ghobadi et al., 2020; Wang et al., 2018), while Swarm can measure gradients at scales larger than several kilometres. We also used the threshold values of scintillation indices to level out noise effects and consider only scintillation events in the analysis (more details in section 2.1). Nevertheless, we do expect an increase of scintillations with the geomagnetic and solar activity and the strength of irregularities, albeit not necessarily linear.

The relationship between irregularities at the Swarm satellites' heights and the scintillation observed from the ground is well present in plots with $\sigma_{\varphi}$ at high latitudes (polar and auroral regions), but not so clearly at low latitudes (Figs. 5, 7, and 9). This can be attributed to the geometry of the geomagnetic field. Despite the high speed of the spacecraft in orbit, scintillation observed from the ground and associated with the *F*-region of the ionosphere and above will also be seen by Swarm as the plasma variations are associated with the same magnetic field line. Plasma density variations in *F*-region extend along the magnetic field lines and thus variations of the ionosphere observed by the ground-based receivers will most likely also be observed by a satellite at high geomagnetic latitudes. At low latitudes, the variations in density can be within a horizontal layer above or below the satellite. However, dependences on the nature of these irregularities also appear well here. For example, in the polar region, the polar cap patches can extend above the ionospheric maximum (Rodger et al., 1994; Lorentzen et al., 2004), so we can see a linear relation in Fig. 5. As mentioned above, the equatorial bubbles (Smith and Heelis, 2017), as well as the peculiarity of the equatorial ionosphere (*G*- and *F3*-layers, Wang et al., 2020), are possible sources of some correlation between the data on the ground and the Swarm satellite (Fig. 9). In the auroral region, particle precipitation down to *E* layer is responsible for observing signal scintillations (Spogli et al., 2009; Prikryl et al., 2011; Jin et al. 2015, 2016). That is why we do not see a clear correlation between the two datasets in Fig. 7 (especially for S4, Fig. 7b).

Various ionospheric irregularities can lead to scintillation. The IPIR index is a product of amplitudes and temporal variations in plasma densities and provides information on the level of ionospheric fluctuations (Jin et al., 2022). We have shown that the IPIR index can be regarded as an indicator of plasma variations, which can lead to scintillation effects (Fig. 10). Detailed comparison of the phase scintillation indices with the IPIR index reveals an increase in the median phase scintillation index values with increasing IPIR index. At the same time, the likelihood of large scintillations increases as well. This allows relating the strength of ionospheric plasma irregularities as reflected in the IPIR index to the impact on *trans*-ionospheric radio signals and the severity of plasma irregularities for the end-users. The results obtained in this study may be re-evaluated in the future by considering more data, including high solar activity levels and by gathering and revising data from extra stations (in the auroral and low latitude regions).

To conclude, we compared the GPS scintillation data measured with 23 ground-based receivers with selected parameters from the IPIR dataset (Jin et al., 2022), in particular the IPIR index. We selected ground stations to represent different ionospheric regions: polar cap and cusp (11 stations), auroral (4 stations), and equatorial regions (8 stations).

1. VTEC data from all considered ground-based stations shows significant linear relations with in-situ electron density and VTEC measured by Swarm.

2. The relation between the ground-based scintillation indices (S4 and $\sigma_{\varphi}$) and the Swarm derived irregularity parameters is not straightforward, since scintillations are the indirect result of irregularities. However, we observe an increase in scintillations with an increase in ionospheric plasma irregularities (positive correlation).
3. The increase in scintillations with increasing plasma irregularities as reflected in the IPIR index allows us to confirm the scale for the IPIR index which reflects the severity of the fluctuations from the user perspective in a statistical sense, indicating the likelihood of scintillations of *trans*-ionospheric radio signals. Thus, the IPIR index can be regarded as an indicator of plasma variations, which can lead to scintillation effects.

## Declaration of Competing Interest

The authors declare that they have no known competing financial interests or personal relationships that could have appeared to influence the work reported in this paper.

## Acknowledgements

This work was supported by the Research Council of Norway grant number 267408, 275653 and it is a part of the 4DSpace Strategic Research Initiative at the University of Oslo. WJM, YJ and DK also acknowledge funding from the European Research Council (ERC) under the European Union's Horizon 2020 research and innovation programme (ERC Consolidator Grant agreement No. 866357, POLAR-4DSpace). We thank the Norwegian Polar Institute for assisting in GPS observations at Ny-Ålesund, and the Tromsø Geophysical Observatory for operating the receiver at Skibotn. We thank the CNR for hosting the GNSS receivers in "Dirigibile Italia" station at Ny-Ålesund, the University of Tromsø for hosting the GNSS receiver in Longyearbyen and SANSA Space Science for hosting the GNSS receiver at SANAE IV station. We thank the Department of Physics at Mbarara University of Science and Technology for supplying the SCINDA data. We also thank the PNRA (Programma Nazionale di Ricerche in Antartide) for supporting the GNSS monitoring at Mario Zucchelli, Concordia and SANAE IV stations and the GRAPE (GNSS Research and Application for Polar Environment) SCAR EG for supporting this study. The scintillation data managed by the Istituto Nazionale di Geofisica e Vulcanologia (INGV) are available at eSWua web portal (www.eswua.ingv.it), that is operated by the Upper Atmosphere Physics and Radio propagation group of INGV.

INGV is grateful to its scientific partners kindly contributing the scintillation data available in eSWua that were used in this study: NAVIS centre of the Hanoi University of Science and Technology (Vietnam), Embry-Riddle Aeronautical University (USA), Pwani University (Kenya), Mackenzie University (Brazil).

We thank Dr. Pierre Cilliers, Dr. Guozhu Li and Dr. DongHe Zhang for providing GPS scintillation data. The Swarm data can be obtained through the official Swarm website ftp://Swarm-diss.eo.esa.int. http://tid.uio.no/plasma/swarm/IPIR_cdf/. The scintillation data from SANAE IV can be accessed via the SANDIMS website https://sandims.sansa.org.za/.

## Appendix A. Supplementary material

Supplementary data to this article can be found online at https://doi.org/10.1016/j.asr.2022.11.042.

## References

Abdu, M.A., Batista, I.S., Carrasco, A.J., Brum, C.G.M., 2005. South Atlantic magnetic anomaly ionization: a review and a new focus on electrodynamic effects in the equatorial ionosphere. J. Atmos. Sol. Terr. Phys. 67, 1643–1657. https://doi.org/10.1016/j.jastp.2005.01.014.

Aol, S., Buchert, S., Jurua, E., 2020. Ionospheric irregularities and scintillations: a direct comparison of in situ density observations with ground-based L-band receivers. Earth Planets Space. 72, 164. https://doi.org/10.1186/s40623-020-01294-z.

Basu, S., Groves, K. M., 2001. Specification and forecasting of outages on satellite communication and navigation systems. In: Song, P., Singer, H.J., Siscoe, G.L. (Eds.) Space Weather. 125, 423–430. https://doi.org/10.1029/GM125p0423.

Basu, S., Basu, S., Mackenzie, E., Fougere, P.F., Coley, W.R., Maynard, N.C., Winningham, J.D., Sugiura, M., Hanson, W.B., Hoegy, W.R., 1988a. Simultaneous density and electric-field fluctuation spectra associated with velocity shears in the auroral oval. J. Geophys. Res. 93 (A1), 115–136. https://doi.org/10.1029/JA093iA01p00115.

Basu, S., Mackenzie, E., Basu, S., 1988b. Ionospheric constraints on VHF/UHF communications links during solar maximum and minimum periods. Radio Sci. 23 (3), 363–378. https://doi.org/10.1029/RS023i003p00363.

Beach, T.L., 2006. Perils of the GPS phase scintillation index ($\sigma\phi$). Radio Sci. 41 (5), RS5S31. https://doi.org/10.1029/2005RS003356.

Bougard, B., Sleewaegen, J.-M., Spogli, L., Veettil, S. V., Monico, J. F., 2011. CIGALA: challenging the solar maximum in Brazil with PolaRxS. In: Proceedings of the ION GNSS 2011, Institute of Navigation, Portland, OR, September 20–23, pp 2572–2579.

Burke, W.J., Huang, C.Y., Valladares, C.E., Machuzak, J.S., Gentile, L. C., Sultan, P.J., 2003. Multipoint observations of equatorial plasma bubbles. J. Geophys. Res. Space Phys. 108 (A5), 1221. https://doi.org/10.1029/2002JA009382.

Carrano, C.S., Anghel, A., Quinn, R.A., Groves, K.M., 2009. Kalman filter estimation of plasmaspheric total electron content using GPS. Radio Sci. 44 (RS0A10). https://doi.org/10.1029/2008RS004070.

Carrano, C.S., Rino, C.L., 2016. A theory of scintillation for two-component power law irregularity spectra: Overview and numerical results. Radio Sci. 51 (6), 789–813. https://doi.org/10.1002/2015RS005903.

Cesaroni, C., Spogli, L., De Franceschi, G., 2021. IONORING: real-time monitoring of the total electron content over Italy. Remote Sens. (Basel) 13 (16), 3290. https://doi.org/10.3390/rs13163290.

Ciraolo, L., Azpilicueta, F., Brunini, C., Meza, A., Radicella, S.M., 2007. Calibration errors on experimental slant total electron content (TEC) determined with GPS. J. Geod. 81 (2), 111–120. https://doi.org/10.1007/s00190-006-0093-1.

Coker, C., Bust, G.S., Doe, R.A., Gaussiran II, T.L., 2004. High latitude plasma structure and scintillation. Radio Sci. 39, RS1S15. https://doi.org/10.1029/2002RS002833.

De Franceschi, G., Spogli, L., Alfonsi, L., Romano, V., Cesaroni, C., Hunstad, I., 2019. The ionospheric irregularities climatology over Svalbard from solar cycle 23. Sci. Rep. 9 (1), 9232. https://doi.org/10.1038/s41598-019-44829-5.

Forte, B., 2005. Optimum detrending of raw GPS data for scintillation measurements at auroral latitudes. J. Atmos. Sol. Terr. Phys. 67 (12), 1100–1109. https://doi.org/10.1016/j.jastp.2005.01.011.

Forte, B., 2007. On the relationship between the geometrical control of scintillation indices and the data detrending problems observed at high latitudes. Ann. Geophys. 50 (6), 699–706. https://doi.org/10.4401/ag-3051.

Forte, B., Radicella, S.M., 2002. Problems in data treatment for ionospheric scintillation measurements. Radio Sci. 37 (6), 1096. https://doi.org/10.1029/2001RS002508.

Fremouw, E.J., Leadabrand, R.L., Livingston, R.C., Cousins, M.D., Rino, C.L., Fair, B.C., Long, R.A., 1978. Early results from the DNA Wideband satellite experiment—Complex-signal scintillation. Radio Sci. 13 (1), 167–187. https://doi.org/10.1029/RS013i001p00167.

Friis-Christensen, E., Lühr, H., Knudsen, D., Haagmans, R., 2008. Swarm–an Earth observation mission investigating geospace. Adv. Space Res. 41 (1), 210–216. https://doi.org/10.1016/j.asr.2006.10.008.

Ghobadi, H., Spogli, L., Alfonsi, L., Cesaroni, C., Cicone, A., Linty, N., et al., 2020. Disentangling ionospheric refraction and diffraction effects in GNSS raw phase through fast iterative filtering technique. GPS Solutions 24, 85. https://doi.org/10.1007/s10291-020-01001-1.

Jayachandran, P.T., Hamza, A.M., Hosokawa, K., Mezaoui, H., Shiokawa, K., 2017. GPS amplitude and phase scintillation associated with polar cap auroral forms. J. Atmos. Sol. Terr. Phys. 164, 185–191. https://doi.org/10.1016/j.jastp.2017.08.030.

Jin, Y., Xiong, C., Clausen, L., Spicher, A., Kotova, D., Brask, S., et al., 2020. Ionospheric plasma irregularities based on in situ measurements from the Swarm satellites e2020JA028103. J. Geophys. Res.: Space Phys. 124. https://doi.org/10.1029/2020JA028103.

Jin, Y., Kotova, D., Xiong, C., Brask, S., Clausen, L.B.N., Kervalishvili, G., Stolle, C., Miloch, W.J., 2022. Ionospheric Plasma IRregularities - IPIR - data product based on data from the Swarm satellites. J. Geophys. Res.: Space Phys. 127. https://doi.org/10.1029/2021JA030183, e2021JA030183.

Jin, Y., Moen, J.I., Miloch, W.J., 2015. On the collocation of the cusp aurora and the GPS phase scintillation: a statistical study. J. Geophys. Res. Space Phys. 120, 9176–9191. https://doi.org/10.1002/2015JA021449.

Jin, Y., Moen, J.I., Miloch, W.J., Clausen, L.B.N., Oksavik, K., 2016. Statistical study of the GNSS phase scintillation associated with two types of auroral blobs. J. Geophys. Res. Space Physics 121, 4679–4697. https://doi.org/10.1002/2016JA022613.

Jin, Y., Moen, J.I., Oksavik, K., Spicher, A., Clausen, L.B.N., Miloch, W. J., 2017. GPS scintillations associated with cusp dynamics and polar cap patches. J. Space Weather Space Clim. 7, A23. https://doi.org/10.1051/swsc/2017022.

Jin, Y., Spicher, A., Xiong, C., Clausen, L.B.N., Kervalishvili, G., Stolle, C., Miloch, W.J., 2019. Ionospheric Plasma Irregularities Characterized by the Swarm Satellites: Statistics at High Latitudes. J. Geophys. Res. Space Phys. 124 (2), 1262–1282. https://doi.org/10.1029/2018JA026063.

Kelley, M.C., 2009. The Earth's Ionosphere Plasma Physics and Electrodynamics, Second Edition. Elsevier, Amsterdam, p. 556.

Keskinen, M.J., Ossakow, S.L., 1983. Theories of high-latitude ionospheric irregularities: a review. Radio Sci. 18, 1077–1091. https://doi.org/10.1029/RS018i006p01077.

Kintner, P.M., Ledvina, B.M., de Paula, E.R., 2007. GPS and ionospheric scintillations. Space Weather 5, S09003. https://doi.org/10.1029/2006SW000260.

Li, G., Ning, B., Otsuka, Y., et al., 2021. Challenges to equatorial plasma bubble and ionospheric scintillation short-term forecasting and future aspects in east and southeast Asia. Surv. Geophys. 42, 201–238. https://doi.org/10.1007/s10712-020-09613-5.

Lorentzen, D.A., Shumilov, N., Moen, J., 2004. Drifting airglow patches in relation to tail reconnection. Geophys. Res. Lett. 31 (2), L02806. https://doi.org/10.1029/2003GL017785.

Mannucci, A.J., Wilson, B.D., Yuan, D.N., Ho, C.H., Lindqwister, U.J., Runge, T.F., 1998. A global mapping technique for GPS-derived ionospheric total electron content measurements. Radio Sci. 33 (3), 565–582. https://doi.org/10.1029/97RS0270.

McCaffrey, A.M., Jayachandran, P.T., 2019. Determination of the refractive contribution to GPS phase "scintillation". J. Geophys. Res. Space Phys. 124 (2), 1454–1469. https://doi.org/10.1029/2018JA025759.

Mushini, S.C., Jayachandran, P.T., Langley, R.B., MacDougall, J.W., Pokhotelov, D., 2012. Improved amplitude-and phase-scintillation indices derived from wavelet detrended high-latitude GPS data. GPS Solutions 16 (3), 363–373. https://doi.org/10.1007/s10291-011-0238-4.

Noja, M., Stolle, C., Park, J., Lühr, H., 2013. Long-term analysis of ionospheric polar patches based on CHAMP TEC data. Radio Sci. 48 (3), 289–301. https://doi.org/10.1002/rds.20033.

Olwendo, J., Cilliers, P., Ming, O., 2019. Comparison of ground based ionospheric scintillation observations with in situ electron density variations as measured by the Swarm satellites. Radio Sci. 54, 852–866. https://doi.org/10.1029/2018rs006734.

Prikryl, P., Jayachandran, P.T., Mushini, S.C., Chadwick, R., 2011. Climatology of GPS phase scintillation and HF radar backscatter for the high-latitude ionosphere under solar minimum conditions. Ann. Geophys. 29 (2), 377–392. https://doi.org/10.5194/angeo-29-377-2011.

Roddy, P.A., Hunton, D.E., Ballenthin, J.O., Groves, K.M., 2010. Correlation of in situ measurements of plasma irregularities with ground-based scintillation observations. J. Geophys. Res. Space Phys. 115, A06303. https://doi.org/10.1029/2010JA015288.

Rodger, A.S., Pinnock, M., Dudeney, J.R., Baker, K.B., Greenwald, R. A., 1994. A new mechanism for polar patch formation. J. Geophys. Res. Space Phys. 99 (A4), 6425–6436. https://doi.org/10.1029/93JA01501.

Skjæveland, A.H., Kotova, D.S., Miloch, W.J., 2021. Case studies of ionospheric plasma irregularities over Queen Maud Land, Antarctica e2021JA029963. J. Geophys. Res.: Space Phys. 126. https://doi.org/10.1029/2021JA029963.

Smith, J., Heelis, R.A., 2017. Equatorial plasma bubbles: variations of occurrence and spatial scale in local time, longitude, season, and solar activity. J. Geophys. Res. Space Phys. 122 (5), 5743–5755. https://doi.org/10.1002/2017JA024128.

Song, K., Meziane, K., Kashcheyev, A., Jayachandran, P.T., 2021. Multifrequency observation of high latitude scintillation: a comparison with the phase screen model. IEEE Trans. Geosci. Remote Sens. 60, 5801209. https://doi.org/10.1109/TGRS.2021.3113778.

Spicher, A., Clausen, L.B.N., Miloch, W.J., Lofstad, V., Jin, Y., Moen, J. I., 2017. Interhemispheric study of polar cap patch occurrence based on Swarm in situ data. J. Geophys. Res. Space Phys. 122, 3837–3851. https://doi.org/10.1002/2016JA023750.

Spogli, L., Alfonsi, L., Franceschi, G.D., Romano, V., Aquino, M.H.O., Dodson, A., 2009. Climatology of GPS ionospheric scintillations over high and mid-latitude European regions. Ann. Geophys. 27 (9), 3429–3437. https://doi.org/10.5194/angeo-27-3429-2009.

Spogli, L., Alfonsi, L., Romano, V., De Franceschi, G., Francisco, G.M. J., Shimabukuro, M.H., et al., 2013. Assessing the GNSS scintillation climate over Brazil under increasing solar activity. J. Atmos. Sol. Terr. Phys. 105, 199–206. https://doi.org/10.1016/j.jastp.2013.10.003.

Spogli, L., Sabbagh, D., Regi, M., Cesaroni, C., Perrone, L., Alfonsi, L., et al., 2021b. Ionospheric response over Brazil to the August 2018 geomagnetic storm as probed by CSES-01 and Swarm satellites and by local ground-based observations e2020JA028368. J. Geophys. Res.: Space Phys. 126 (2). https://doi.org/10.1029/2020JA028368.

Spogli, L., Ghobadi, H., Cicone, A., Alfonsi, L., Cesaroni, C., Linty, N., et al., 2021. Adaptive phase detrending for GNSS scintillation detection: a case study over Antarctica. IEEE Geosci. Remote Sens. Lett. 19, 8009905. https://doi.org/10.1109/LGRS.2021.3067727.

Stolle, C., Floberghagen, R., Lühr, H., et al., 2013. Space Weather opportunities from the Swarm mission including near real time applications. Earth Planet Sp 65, 17. https://doi.org/10.5047/eps.2013.10.002.

Upper atmosphere physics and radiopropagation Working Group, Cesaroni C., De Franceschi G., Marcocci C., Pica E., Romano V., Spogli L. (2020). Electronic Space Weather upper atmosphere database (eSWua) - GNSS scintillation data, version 1.0. Istituto Nazionale di Geofisica e Vulcanologia (INGV). https://doi.org/10.13127/eswua/gnss (data of access: 18.11.2022).

Van Dierendonck, A. J., Klobuchar, J., Quyen, H., 1993. Ionospheric Scintillation monitoring using commercial single frequency C/A code receivers. In: Proceedings of the ION GPS 1993, Institute of Navigation, Salt Lake City, UT, September 22–24, pp 1333–1342.

Wang, X., Cheng, W., Zhou, Z., Yang, D., Cui, J., Guo, F., 2020. Stratification observed by the in situ plasma density measurements from the Swarm satellites. Ann. Geophys. 38, 517–526. https://doi.org/10.5194/angeo-38-517-2020.

Wang, Y., Zhang, Q.H., Jayachandran, P.T., Moen, J., Xing, Z.Y., Chadwick, R., et al., 2018. Experimental evidence on the dependence of the standard GPS phase scintillation index on the ionospheric plasma drift around noon sector of the polar ionosphere. J. Geophys. Res. Space Phys. 123 (3), 2370–2378. https://doi.org/10.1002/2017JA024805.

Wernik, A.W., Secan, J.A., Fremouw, E.J., 2003. Ionospheric irregularities and scintillation. Adv Space Res 31 (4), 971–981. https://doi.org/10.1016/S0273-1177(02)00795-0.

Whittaker, I.C., Gamble, R.J., Rodger, C.J., Clilverd, M.A., Sauvaud, J.-A., 2013. Determining the spectra of radiation belt electron losses: Fitting DEMETER electron flux observations for typical and storm times. J. Geophys. Res. Space Physics 118, 7611–7623. https://doi.org/10.1002/2013JA019228.

Wood, A.G., Alfonsi, L., Clausen, L.B.N., Jin, Y., Spogli, L., Urbar, J., Rawlings, J.R., Whittaker, I.C., Dorrian, G.D., Høeg, P., Kotova, D., Cesaroni, C., Cicone, A., Miedzik, J., Gierlach, E., Kochanska, P., Wojtkiewicz, P., Shahtahmassebi, G., Miloch, W.J., 2022. Variability of Ionospheric Plasma: Results from the ESA Swarm Mission. Space Sci. Rev. 218, 52. https://doi.org/10.1007/s11214-022-00916-0.

Yasyukevich, A.S., Vesnin, A.M., Yasyukevich, Y.V., Padokhin, A.M., 2019. Correlation between Total and Plasmasphere Electron Content and Indexes of Solar and Geomagnetic Activity. In: Proceedings of the 2019 Russian Open Conference on Radio Wave Propagation (RWP), Kazan Federal University, Kazan, Russia, July 1-6, IEEE, pp 87-90. doi: 10.1109/RWP.2019.8810364.

Yeh, K.-C., Liu, C.-H., 1982. Radio Wave Scintillations in the Ionosphere. Proc. IEEE 70, 324–360. https://doi.org/10.1109/PROC.1982.12313.